NEDD4 regulates VEGF signaling and mTOR to promote angiogenesis and the cell cycle in steroid-induced osteonecrosis of the femoral head

JIAN LI[1], DONG ZHEN[1], YUHUAN QIN[1] and CAIFEN GUO[2]

[1]Department of Sports Medicine, The Beijing Jishuitan Hospital Guizhou Hospital, Guiyang, Guizhou 550014, P.R. China;
[2]Department of Urology, The Affiliated Hospital of Guizhou Medical University, Guiyang, Guizhou 550004, P.R. China

Received July 8, 2025; Accepted October 17, 2025

DOI: 10.3892/mmr.2025.13759

Abstract. Steroid-induced osteonecrosis of the femoral head (SONFH) is a progressive hip condition marked by osteocyte apoptosis from poor blood supply, leading to femoral head collapse and hip joint dysfunction. Examination of the GSE123568 dataset revealed the important role of ubiquitination in the development of SONFH, contributing to processes such as 'apoptosis', 'protein processing in the endoplasmic reticulum', 'lysosome function', 'cell cycle regulation and autophagy'. The present research revealed that the E3 ubiquitin ligase neural precursor cell expressed developmentally downregulated protein 4 (NEDD4) is involved in SONFH, showing positive correlations with key genes in the p53 signaling pathway, DNA damage response and cell cycle regulation. This highlights the role of NEDD4 in DNA repair and cell cycle control. Additionally, NEDD4 exhibited varying regulatory effects on integrin, TGF-β/SMAD, Hippo/yes-associated protein and Notch signaling pathways, underscoring its multifaceted role in cellular signaling. A NEDD4 overexpression vector was created and found to significantly boost the viability, migration and angiogenesis of bone microvascular endothelial cells (BMECs). Reverse transcription-quantitative PCR results revealed higher mRNA levels of mTOR, VEGF and VEGFR2 in NEDD4-overexpressing cells, suggesting that the VEGF signaling pathway was activated. Immunoprecipitation assays showed decreased mTOR ubiquitination levels following NEDD4 overexpression, suggesting NEDD4 may indirectly modulate mTOR ubiquitination rather than directly catalyzing it., Small interfering RNA experiments found that NEDD4 and mTOR cooperated to boost BMEC proliferation and migration, as confirmed by MTT, EdU and wound healing assays. Furthermore, the present research showed that glucocorticoids could suppress NEDD4 expression by increasing promoter methylation levels. These findings highlight the key roles of NEDD4 in angiogenesis, maintaining cell balance, regulating the cell cycle and repairing DNA damage in SONFH. By demonstrating the numerous functions of NEDD4 in steroid-induced osteonecrosis and angiogenesis, the present study suggested that it may impact vascular growth and bone tissue repair through multiple pathways and mechanisms.

Correspondence to: Dr Caifen Guo, Department of Urology, The Affiliated Hospital of Guizhou Medical University, 28 Guiyi Street, Yunyan, Guiyang, Guizhou 550004, P.R. China
E-mail: gcf0213@163.com

Key words: neural precursor cell expressed developmentally downregulated protein 4, steroid-induced osteonecrosis of the femoral head, bone microvascular endothelial cells, angiogenesis

Introduction

Osteonecrosis of the femoral head (ONFH) is a degenerative hip joint disease that worsens over time (1). ONFH is characterized by bone cell death due to a lack of blood supply, which can lead to joint collapse and hip dysfunction (1). The causes of ONFH are complex and involve mechanical injury, genetic predisposition and biochemical imbalances (2,3). Among these factors, steroid use is reported in ~51% of ONFH cases (4). Prolonged or high-dose steroid therapy markedly increases the risk of ONFH, leading to steroid-induced ONFH (SONFH) (1). For example, in patients with systemic lupus erythematosus, the corticosteroid dosage is positively associated with the occurrence of ONFH. Daily doses as low as 10 mg have been associated with a 3.6% increase in risk, while doses >40 mg greatly increase the chance of developing ONFH (5). Steroids damage bone and blood vessel health through various mechanisms, including endothelial cell dysfunction and reduced angiogenesis, ultimately impairing blood flow supply (3,6). Endothelial cells serve an important role in angiogenesis, as their growth, migration and tube formation are important for repairing bone tissue (6,7). When angiogenesis is impaired, bone regeneration often fails (8). VEGF, a key factor that promotes angiogenesis, has been shown to enhance bone repair by stimulating angiogenesis, making it a potential treatment for ONFH (9-11). Angiogenesis and osteogenesis are closely linked processes that occur throughout bone development, maturation, aging and disease progression (12). Notably, activation of the VEGF-Notch signaling pathway has been reported to restore the proliferation of mesenchymal stem cells in aplastic anemia (13), while the mTOR/AP-1

complex subunit μ-1/VEGF axis regulates endothelial cell growth (14). Additionally, increasing hypoxia-inducible factor (HIF)-1α/VEGF levels can help to protect against bone loss in models of nasal obstruction (15). Therefore, understanding the molecular mechanisms of angiogenesis and endothelial cell function is important for advancing treatments for ONFH.

Ubiquitination has become an important post-translational modification for regulating protein stability, signal transduction and cellular homeostasis (16-19). Neural precursor cell expressed developmentally downregulated protein 4 (NEDD4) is an E3 ubiquitin ligase that facilitates substrate ubiquitination and degradation, thereby influencing multiple biological processes such as cell proliferation, migration, angiogenesis and endothelial cell protection (20-22). NEDD4 has been demonstrated to promote endothelial cell proliferation, migration and angiogenesis (23). In addition to its role in endothelial regulation, NEDD4 also affects macrophage autophagy and tumor cell proliferation, highlighting its versatile function in maintaining the cellular balance (21,24).

NEDD4 subfamily influences osteogenesis and bone cell biology (25). By mediating PTEN degradation, NEDD4 activates the PI3K/AKT pathway, which promotes cell proliferation and survival. This pathway also supports angiogenesis through PTEN inactivation and VEGF upregulation (26-29). Additionally, NEDD4 boosts osteocyte proliferation and is associated with improved outcomes in postmenopausal osteoporosis (30,31). Overall, these findings emphasize the potential of NEDD4 as a regulator of both angiogenesis and osteogenesis, making it a promising target in ONFH therapy. The present study was based on the concept that NEDD4 may serve a role in SONFH. To explore this, the present study observed how overexpression of NEDD4 affected the viability, migration and tube formation of bone microvascular endothelial cells (BMECs). The present study also investigated how glucocorticoids influenced NEDD4 expression and promoter methylation, shedding light on how NEDD4 contributes to angiogenesis and repair in SONFH.

Materials and methods

Construction of the NEDD4 overexpression (OE) vector. Plasmids pcDNA3.1-NEDD4-3xHA (cat. no. HG-HO284338; HonorGene Biotechnology Co., Ltd.) and the negative control (NC) were transformed into competent *E. coli* cells (AoLu Biotechnology Co., Ltd.). A total of 2 μl plasmid was combined with 100 μl competent cells, on ice for 30 min. The mixture was heat-shocked at 42˚C for 90 sec and cooled on ice for 3 min. Subsequently, 700 μl LB (Luria-Bertani) medium (cat. no. L3022; Thermo Fisher Scientific, Inc.) was added, and the mixture was incubated at 37˚C with shaking at 200 x g for 1 h. This was followed by plating 60 μl cells onto LB agar containing ampicillin (Amp) and incubation at 37˚C for 12-14 h. A single colony was selected and inoculated into 20 ml LB medium with 50 μg/ml Amp, followed by incubation overnight at 37˚C. Subsequently, the culture was scaled up in 50 ml LB/Amp medium and incubated for 12-16 h. Plasmids were extracted using the HiBind DNA plasmid extraction kit (Omega Bio-Tek, Inc.) according to the manufacturer's protocol. DNA concentration was determined using an Implen NanoPhotometer (Implen GmbH) and the sequence was verified by Sanger sequencing (performed by AoNuo Gene Technology Co., Ltd.). The purified plasmids were used for cell transfection at a final amount of 2 μg DNA per well in a 6-well plate, mixed with 6-8 μl PEI-40K transfection reagent (Wuhan Servicebio Technology Co., Ltd.) and incubated at room temperature for 15 min before being added to BMECs. Cells were cultured at 37˚C, 5% CO_2 for 5 h, then refreshed with complete medium and harvested 48 h post-transfection for subsequent experiments. OE-NC consisted of the corresponding empty vector backbone (pcDNA3.1 empty vector; cat. no. V79020; Thermo Fisher Scientific, Inc.), ensuring that any observed effects were specifically attributable to NEDD4 OE. siRNA sequences, including the NC, are listed in Table SI. The purified plasmids were used for transfection at a final amount of 2 μg DNA per well in a 6-well plate.

Transient transfection of BMECs. For the present study, BMECs were obtained from AoLu Biotechnology Co., Ltd. (cat. no. ORC0562). BMECs were seeded at a density of $6x10^5$ cells per well in 6-well plates. BMECs were cultured in complete Endothelial Cell Medium (ScienCell Research Laboratories) supplemented with 10% fetal bovine serum (FBS) and 1% penicillin-streptomycin (100 U/ml and 100 μg/ml, respectively; all Gibco; Thermo Fisher Scientific, Inc.) at 37˚C. After washing with PBS twice, cells were cultured in 1.8 ml serum-free basal medium (Endothelial Cell Medium). To prepare the transfection complexes, solution A, consisting of 100 μl serum-free medium with 20 nM siRNA, was mixed with solution B comprising 100 μl serum-free medium with 6-8 μl PEI 40K (Wuhan Servicebio Technology Co., Ltd.). Subsequently, this mixture was added dropwise to each well. The cells were incubated at 37˚C for 5 h. The cells were harvested 48 h after transfection for subsequent experiments. Cells were centrifuged at 200 x g for 5 min at 4˚C, resuspended in Cell Freezing Medium; Gibco; cat. no. 12648010), transferred to cryovials and stored at -80˚C overnight before being transferred to liquid nitrogen for long-term storage.

Reverse transcription-quantitative PCR (RT-qPCR). BMECs were divided into eight groups: OE-NC, OE-NEDD4, control, si-NEDD4, si-mTOR-1, si-mTOR-2, si-mTOR-3 and si-NEDD4 + si-mTOR. Total RNA was isolated using TRIzol reagent (Thermo Fisher Scientific, Inc.). according to the manufacturer's protocol. The quality and concentration of the RNA were then determined spectrophotometrically. First-strand cDNA synthesis was performed using the SureScript First-Strand cDNA Synthesis Kit (Wuhan Servicebio Technology Co., Ltd.). qPCR was performed with SYBR Green Master Mix (Takara Bio, Inc.) on a StepOnePlus™ Real-Time PCR System (Bio-Rad Laboratories, Inc.). RT was performed at 42˚C for 15 min, followed by 85˚C for 5 sec. qPCR thermocycling conditions were as follows: initial denaturation at 95˚C for 30 sec, followed by 40 cycles of 95˚C for 5 sec and 60˚C for 30 sec. Relative mRNA expression was calculated using the $2^{-\Delta\Delta Cq}$ method (32). The primers used are listed in Table SII. GAPDH was used as the reference gene.

Western blot analysis of NEDD4 expression. Cells were harvested 48 h after transfection with si-NEDD4, pcDNA3.1-NEDD4-3xHA or the respective controls. Total

proteins were extracted using RIPA lysis buffer (Beyotime Biotechnology) supplemented with protease inhibitors (cat. no. 78430; Thermo Fisher Scientific, Inc.). Protein concentrations were quantified using the BCA Protein Assay Kit (cat. no. 23225; Thermo Fisher Scientific, Inc.). Equal quantities of protein (20-30 μg/lane) were separated via 8-10% SDS-PAGE and subsequently transferred onto PVDF membranes (MilliporeSigma). Membranes were blocked with 5% BSA (Beijing Solarbio Science & Technology Co., Ltd.) for 1 h at room temperature, followed by overnight incubation at 4˚C with the following primary antibodies: Anti-NEDD4 (1:2,000; cat. no. AF4636; Affinity Biosciences) and anti-β-actin (1:25,000; cat. no. 66009-1-Ig; Proteintech Group, Inc.) as the loading control. After washing with TBST (0.1% Tween-20), membranes were incubated with HRP-conjugated secondary antibodies: Goat anti-rabbit IgG (H+L) (1:3,000; cat. no. GB23303; Wuhan Servicebio Technology Co., Ltd.) and goat anti-mouse IgG (H+L) (1:5,000; cat. no. GB23301; Wuhan Servicebio Technology Co., Ltd.) for 1 h at room temperature. Protein bands were visualized using the Pierce ECL Western Blotting Substrate (Thermo Fisher Scientific, Inc.) and band intensities were semi-quantified using ImageJ software (version 1.53; National Institutes of Health).

MTT assay. Cells were incubated in 90 μl DMEM/F12 (Meilunbio) supplemented with 10% FBS and 1% penicillin-streptomycin with 10 μl 5 mg/ml MTT solution (Beijing Solarbio Science & Technology Co., Ltd.) for 4 h. The supernatants were then removed, and 110 μl DMSO formazan solubilization solution was added. The absorbance was measured at 560 nm using a Bio-Rad microplate reader.

5-ethynyl-2'-deoxyuridine (EdU) proliferation assay. Cell proliferation was evaluated using the EdU Cell Proliferation Kit (Wuhan Servicebio Technology Co., Ltd.) according to the manufacturer's instructions. In brief, cells from various experimental groups were seeded into 24-well plates at a density of $1x10^5$ cells/well and incubated with EdU working solution for 2 h at 37˚C. After fixation with 4% paraformaldehyde (Beijing Solarbio Science & Technology Co., Ltd.) at room temperature for 15 min and permeabilization with 0.5% Triton X-100, cells were stained using the Apollo® 567 fluorescent dye at room temperature for 30 min, according to the manufacturer's instructions.. Images were captured using a Nikon fluorescence microscope (Nikon Corporation) Cells that incorporated nuclear EdU exhibited green fluorescence. The percentage of EdU-positive cells was calculated from five randomly chosen fields per group and the data were statistically analyzed using ImageJ software (version 1.53; National Institutes of Health).

Tube formation assay. Matrigel® (150 μl/well; Corning, Inc.) was added to 48-well plates and allowed to solidify at 37˚C for 30 min. Cells ($1x10^5$/well) were then seeded and incubated at 37˚C for 4 h. Cells were stained with Calcein-AM (2 μM; Beyotime Biotechnology) at 37˚C for 30 min to visualize the tubular network. The formation of tubes was observed and images were captured under an inverted fluorescence microscope (Motic Biological Technology Co., Ltd.).

Wound healing assay. BMECs were seeded into 6-well plates in triplicate and cultured until reaching 100% confluence. Cells were serum-starved overnight prior to the assay. Cells were cultured in DMEM/F12 with 10% fetal bovine serum (Gibco, USA) and 1% penicillin-streptomycin. A linear scratch was created across the cell monolayer using a sterile 200-μl pipette tip. Detached cells were removed by rinsing the wells three times with PBS, after which fresh culture medium containing NEDD4 overexpression plasmid, si-NEDD4 and their respective negative controls. Images were captured at 0, 24 and 48 h using an inverted light microscope (Motic Biological Technology Co., Ltd.). The scratch width was measured in pixels using ImageJ software (version 1.53; National Institutes of Health), with the width at 0 h defined as 100% (baseline); the widths at subsequent time points were expressed as a percentage relative to this baseline. The mean value from three independent experiments was used for analysis.

Methylation-specific PCR. Genomic DNA was extracted from BMECs using a DNA extraction kit (Omega Bio-Tek, Inc.) and then converted to bisulfite using the EZ DNA Methylation-Gold Kit (Zymo Research Corp.). The methylation status was detected through PCR using Taq DNA Polymerase (Takara Bio, Inc.) with the following primers: NEDD4-M (methylated): Forward, 5'-ATTTTTTGTAGAAAGATTTGAAGGC-3' and reverse, 5'-CGCAACTCTATAATTAAATTTAACGAT-3'; NEDD4-U (unmethylated): Forward, 5'-TTTTTGTAGAAA GATTTGAAGGTGT-3' and Reverse, 5'-CACAACTCTATA ATTAAATTTAACAAT-3'. The thermocycling conditions were as follows: Initial denaturation at 95˚C for 5 min, followed by 40 cycles of 95˚C for 30 sec, 58˚C for 30 sec and 72˚C for 30 sec and final extension at 72˚C for 10 min. PCR products were separated on 2% agarose gels and visualized using an E-Gel Imager system (Thermo Fisher Scientific, Inc.) with ethidium bromide staining The experiment included five groups as follows: i) H_2O (blank negative control); ii) BMECs treated with PBS (vehicle control); iii) BMECs treated with 1 μM methylprednisolone (MePr; MedChemExpress); iv) BMECs treated with 5 μM 5-azacytidine (5-AZA; Sigma-Aldrich; Merck KGaA); and v) BMECs co-treated with MePr (1 μM) and 5-AZA (5 μM). All treatments were performed at 37˚C for 48 h under standard cell-culture conditions.

Immunoprecipitation (IP) assay. Proteins were extracted from the cells using RIPA buffer (Beyotime Biotechnology; cat. no. P0013B) that contained a protease inhibitor cocktail (cat. no. 04693132001; Roche Diagnostics). The cell lysates were then cleared by centrifugation at 12,000 x g for 15 min at 4˚C. The protein concentrations were measured using a BCA Protein Assay Kit (cat. no. 23225; Thermo Fisher Scientific, Inc.). A total of 500 μg lysate (300 μl) was incubated with Protein A/G magnetic beads (50 μl; cat. no. 88802; Thermo Fisher Scientific, Inc.) prebound to anti-ubiquitin antibody (2 μg; 1:2,000; cat. no. ER65617; Hangzhou HuaAn Biotechnology Co., Ltd.) overnight at 4˚C. Beads were washed three times with cold PBS containing 0.1% Tween-20, followed by centrifugation at 2,000 x g for 3 min at 4˚C. The immunocomplexes were eluted by boiling for 5 min in SDS loading buffer (Beyotime Institute of Biotechnology). Subsequently, 30 μg of total protein per lane

was separated using 8-10% SDS-PAGE, transferred onto PVDF membranes, and blocked with 5% BSA (Servicebio) for 1 h at room temperature. Membranes were incubated with primary antibodies overnight at 4˚C, followed by 1 h incubation with secondary antibodies at room temperature, and then incubated with the following primary antibodies:, anti-mTOR (1:20; cat. no. AF6308; Affinity Biosciences); anti-ubiquitin (1:2,000; cat. no. ER65617; Hangzhou HuaAn Biotechnology Co., Ltd.). This was followed by incubation with HRP-conjugated goat anti-rabbit IgG (H+L) (1:3,000; cat. no. GB23303; Servicebio);Goat anti-mouse IgG (H+L) (1:5,000; cat. no. GB23301; Servicebio) ,and visualization using ECL reagents (Thermo Fisher Scientific, Inc.). Images of bands were captured the ChemiDoc™ Touch Imaging System (cat. no. 1708370; Bio-Rad Laboratories, Inc.) and band intensities were semi-quantified using ImageJ software version 1.54 (National Institutes of Health). Statistical analysis was carried out using GraphPad Prism 8 (Dotmatics). Western blotting was performed as aforementioned.

Bioinformatics analysis. The GSE123568 dataset (33) from the Gene Expression Omnibus (GEO) database (ncbi.nlm.nih.gov/geo/), which includes gene expression profiles from 30 patients with SONFH and 10 controls, was analyzed. Differential expression analysis was performed using the 'limma' package (v3.58.1; bioconductor.org/packages/limma/) in R software (version 4.3.2; R Foundation for Statistical Computing, Vienna, Austria), with the cut-off criteria of |log2FC| ≥1 and adjusted P<0.05. Additional analyses included weighted gene co-expression network analysis (WGCNA; version 1.72-5; horvath.genetics.ucla.edu/html/CoexpressionNetwork/), single-sample Gene Set Enrichment Analysis (ssGSEA; GSVA version 1.46.0; https://bioconductor.org/packages/GSVA/), and random forest and support vector machine (SVM) modeling (MetaboAnalyst version 4.0.0; https://www.metaboanalyst.ca/). Principal component analysis (PCA) was performed using the 'FactoMineR' package (version 2.8; https://cran.r-project.org/package=FactoMineR) to visualize sample clustering. Enrichment analysis was conducted using the Kyoto Encyclopedia of Genes and Genomes (KEGG) Orthology Based Annotation System (http://bioinfo.org/kobas/) Gene Ontology (GO) annotation. Protein–protein interaction networks were constructed using STRING (version 12.0; string-db.org/). Pathway enrichment analysis was performed using the REACTOME database (reactome.org/). All data visualization was performed in R using the 'ggplot2' package (version 3.5.1; cran.r-project.org/package=ggplot2).

Receiver operating characteristic (ROC) curve analysis was performed using the pROC package in R to evaluate the diagnostic performance of key ubiquitination-related genes and multivariate predictive models.

Gene selection frequencies were calculated as the number of times each gene was identified as an important variable across repeated resampling steps during model training.

The present study retrieved the gene expression dataset GSE123568 from the GEO database, a publicly available functional genomics repository. This dataset was created using the GPL15207 Affymetrix Human Gene Expression Array platform (Thermo Fisher Scientific, Inc.) and contained peripheral blood mononuclear cell samples from 40 individuals, including 30 patients with SONFH and 10 controls without SONFH. For more details on clinical information and experimental protocols, please refer to the original submission. In the present study, the dataset was used to analyze differential gene expression and then subjected to bioinformatics techniques such as functional enrichment and network analysis to pinpoint candidate genes and signaling pathways associated with SONFH.

Statistical analysis. Data are presented as the mean ± standard error of the mean. The data were analyzed using GraphPad Prism 8 (Dotmatics). For comparisons between two groups, unpaired Student's t-tests were used. For comparisons among multiple groups, one-way ANOVA was performed followed by Tukey's multiple comparisons test as the post hoc test. Pearson's correlation test was performed to evaluate association between gene expression levels. All experiments were independently repeated ≥3 times to ensure reproducibility. All statistical analyses included the necessary corrections for multiple testing using the Benjamini-Hochberg false discovery rate method. P<0.05 was considered to indicate a statistically significant difference.

Results

Changes in gene expression after SONFH are closely associated with ubiquitination in terms of functional enrichment. The principal component (PC) analysis performed on the GSE123568 dataset revealed partial separation between the control group and the SONFH group, with notable separation in PC1 and PC2, highlighting notable differences in gene expression patterns (Fig. 1A). Analysis of differential gene expression revealed 229 upregulated genes and 349 downregulated genes, with significant differences in TSTA3, RIOK3, STOM, HEPACAM2, RUNX2, ARAP1, TYK2 and SIGLEC7 (Fig. 1B). KEGG enrichment analysis revealed pathways that were significantly enriched, including, 'protein processing in endoplasmic reticulum', 'lysosome', 'cell cycle' and 'autophagy-animal'. The enriched REACTOME pathways included 'Deubiquitination' and 'Antigen processing: Ubiquitination & Proteasome degradation'. Gene Ontology (GO) enrichment analysis showed significant enrichment in processes related to ubiquitination, such as 'proteasome mediated ubiquitin dependent protein catabolic process', 'ubiquitin protein ligase activity', 'ubiquitin-dependent protein catabolic process', 'protein polyubiquitination', 'ubiquitin ligase complex', 'ubiquitin conjugating enzyme binding', 'positive regulation of ubiquitin-protein transferase activity' and 'protein deubiquitination'. These findings indicated significant differences in gene expression and biological functions between the SONFH and control groups, particularly in pathways related to ubiquitination (Fig. 1C).

Association of ubiquitination with SONFH. To investigate the role of ubiquitination in SONFH, ssGSEA was first performed on pathways related to ubiquitination, cell proliferation and the cell cycle using the KEGG, GO and REACTOME databases. This revealed marked differences in scores between the control and SONFH groups (Fig. S1). Subsequently, key ubiquitination-related pathway ssGSEA

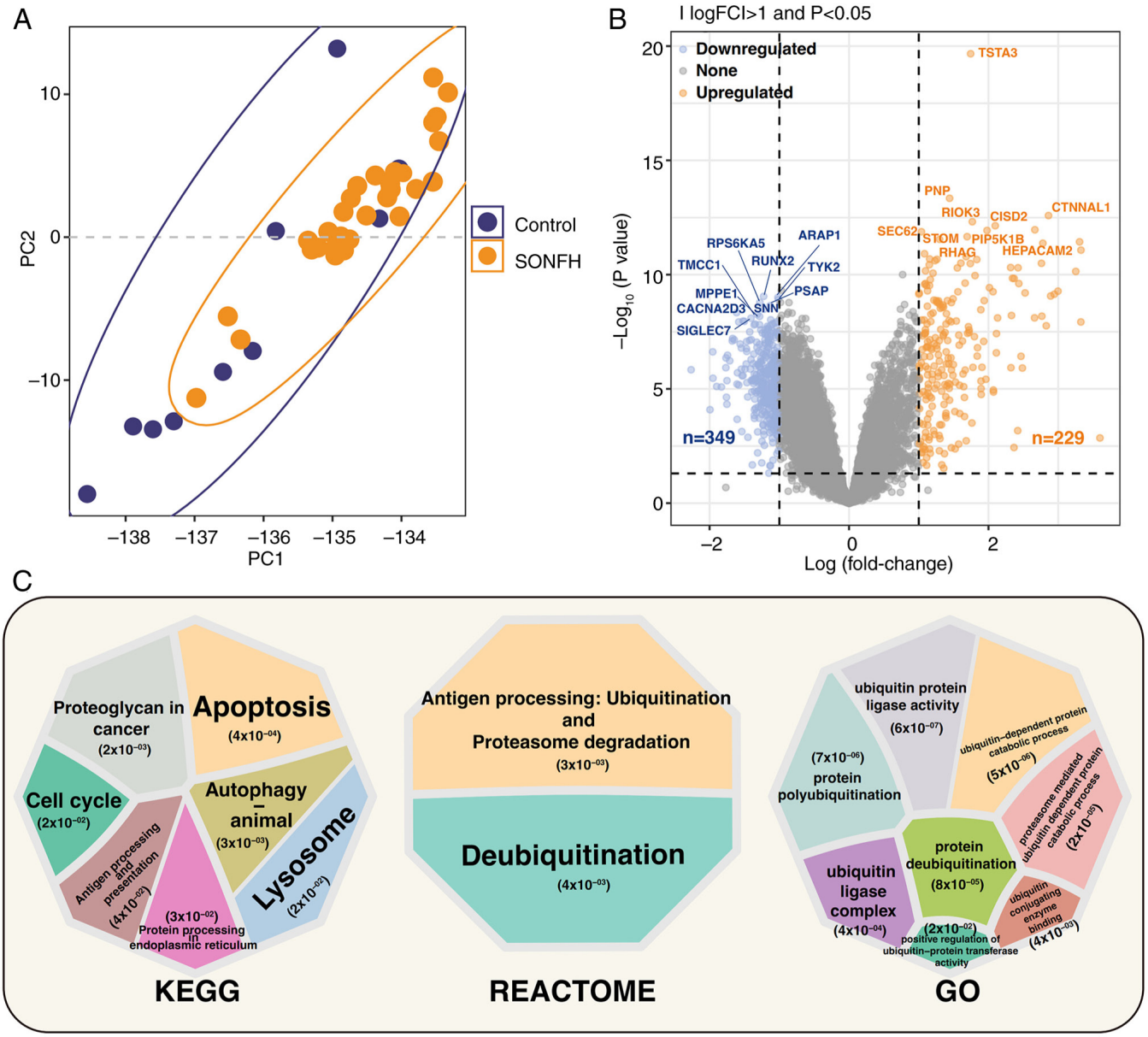

Figure 1. Differential gene and pathway enrichment analysis between the control and SONFH groups. (A) PC analysis showing the separation between control and SONFH groups. (B) Results of differential analysis. The x-axis represents log(fold change) and the y-axis represents-$\log_{10}$ (P-value). Differentially expressed genes are categorized as upregulated, downregulated or not significantly changed. Genes with |log(FC)|>1 and P<0.05 were considered significantly differentially expressed (orange for upregulated, blue for downregulated and gray for not significantly changed). (C) KEGG, REACTOME and GO enrichment results, with significant pathways highlighted. The pathways were selected based on P<0.05 and |log(FC)| >1). Each circle represents one pathway; the size of the circle corresponds to the number of genes, while the color indicates-$\log_{10}$ (P-value), with darker colors representing higher significance. SONFH, steroid-induced osteonecrosis of the femoral head; KEGG, Kyoto Encyclopedia of Genes and Genomes; GO, Gene Ontology; FC, fold change; PC, principal component.

scores were chosen for co-expression network analysis, using control and SONFH as phenotypes in WGCNA. Numerous module pathways, including those associated with ubiquitination, angiogenesis and cell proliferation, exhibited significant differences between the SONFH and control phenotypes (Fig. 2A and B). Genes from 489 pathways in the ME (module eigengene (ME) pink module were selected for network interaction analysis, identifying UBB and UBC at the core of the network (Fig. 2C). Further analysis showed the effect of ubiquitination on SONFH. Using ssGSEA scores from ubiquitination-related pathways as phenotypes, WGCNA was performed again, revealing significant roles for these pathways in different gene modules. In the MEdarkgrey module, pathways such as 'positive regulation of protein ubiquitination' (R=0.47), 'ubiquitin mediated proteolysis' (R=0.77) and 'ubiquitin-ubiquitin ligase activity' (R=0.41) exhibited significant correlations with module genes (Fig. 2D and E). Network interaction analysis revealed the interactions between these genes in the context of ubiquitination, with RNF213, TTN, FSIP2, KIAA1109 and UBR4 at the network center (Fig. 2F), and demonstrated that the E3 ubiquitin ligase NEDD4 was connected to two core network genes, RNF213 and FSIP2, within the ubiquitination-associated network.

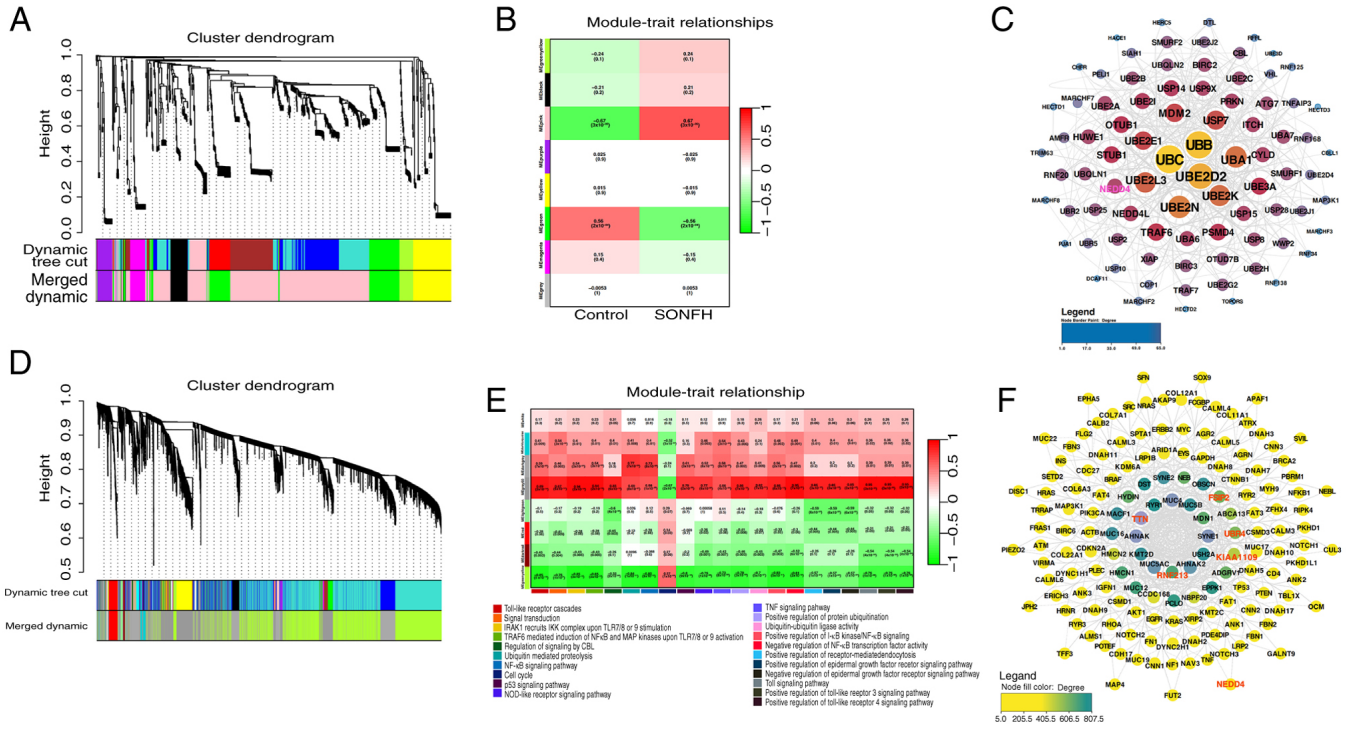

Figure 2. Weighted gene co-expression network analysis. (A) Cluster dendrogram of involved pathways. (B) Heatmap showing correlations between MEs) and the control and SONFH groups, with correlation coefficients and P-values shown in rectangles and parentheses, respectively. (C) Pathway gene interaction network in the MEpink module, with circle size and color indicating degree values. (D) Clustering dendrogram of involved genes, showing modules containing pathways significantly associated with ME. (E) Heatmap of ME correlations with pathways. (F) Gene interaction network in the MEdarkgrey module. SONFH, steroid-induced osteonecrosis of the femoral head; ME, module eigengene.

Role of NEDD4 in ubiquitination related to SONFH. The next step was to investigate genes closely associated with ubiquitination pathways in SONFH. The present study used multivariate exploratory receiver operating characteristic (ROC) analysis on specific pathway genes to achieve this. In the ubiquitin-ubiquitin ligase activity pathway, the two-factor model achieved an AUC of 0.876 and a predictive accuracy of 87.3% (Fig. 3A, right), indicating a strong ability to distinguish between the control and SONFH groups. The five-factor model was demonstrated to be the most accurate predictor, with an AUC value of 0.876. Here, gene selection frequency reflects the relative stability and importance of each gene during model construction .Gene selection frequencies were ranked from highest to lowest as follows: SIAH2, BIRC2, MIB2, RNF128, ZNRF1, RBX1, WWP2, NEDD4L, NEDD4, BIRC3, CBL, UBR2, WWP1, SMURF1 and HUWE1 (Fig. 3A). Within the ubiquitin-mediated proteolysis pathway, all AUC values were >0.8, with the two-factor model yielding the highest AUC at 0.935. Gene selection frequencies, ranked from highest to lowest, were: UBE2F, HERC2, BRCA1, NEDD4, UBE2N, UBE2B and VHL (Fig. 3B). In the positive regulation of protein ubiquitination pathway, ROC curves exhibited AUC values >0.75, indicating high sensitivity. The 10-factor model demonstrated high specificity and accuracy, with an AUC of 0.893. Gene selection frequencies, ranked from highest to lowest, were: UBE2D1, ANKRD13A, CUL1, SIAH1, TRIM21, TRAF6, BIRC2, FBXW7, HUWE1, UBE2N, UBE3A, SKP2, STUB1, NEDD4 and RNF8 (Fig. 3C). ROC analysis revealed that NEDD4 had high AUC values and high selection frequencies across multiple pathways, especially in the ubiquitin-ubiquitin ligase activity and ubiquitin-mediated proteolysis pathways. This suggested a significant role for NEDD4 in distinguishing between control and SONFH groups. Gene contribution analysis, random forest analysis and SVM analyses also supported this finding (Fig. S2). NEDD4 consistently ranked among the top genes by feature importance, accuracy contribution and selection frequency, underscoring its robust predictive value.

NEDD4 potentially regulates the cell cycle, angiogenesis and cell proliferation in SONFH. Based on the analyses showing the potential regulatory role of NEDD4 in SONFH, correlation analyses were performed. The results of the present study revealed significant associations between NEDD4 and pathways related to the cell cycle, angiogenesis and cell growth. Specifically, NEDD4 was negatively correlated with key pathways, including the 'HIF-1 signaling pathway' (R=-0.37), 'integrin signaling pathway' (R=-0.42) and 'Notch signaling pathway' (R=-0.49). Additionally, NEDD4 was positively correlated with multiple pathways, including the 'p53 signaling pathway' (R=0.43), 'DNA damage response pathway' (R=0.45) and the 'G_2/M transition regulation pathway' (R=0.51; Fig. 4A). Among cell cycle-related genes, NEDD4 showed significant positive correlations with key genes such as WEE1 (R=0.51), CCNE1 (R=0.45), MSH6 (R=0.54), ERCC1 (R=0.60), CDK6 (R=0.54) and CENPF (R=0.57), further supporting the role of NEDD4 in regulating the cell cycle (Figs. 4B and S3). NEDD4 also showed positive correlations with multiple angiogenesis-associated genes, including ANGPT2 (R=0.50), VEGFB (R=0.33) and FERMT2 (R=0.59), suggesting a potential role for NEDD4 in regulating

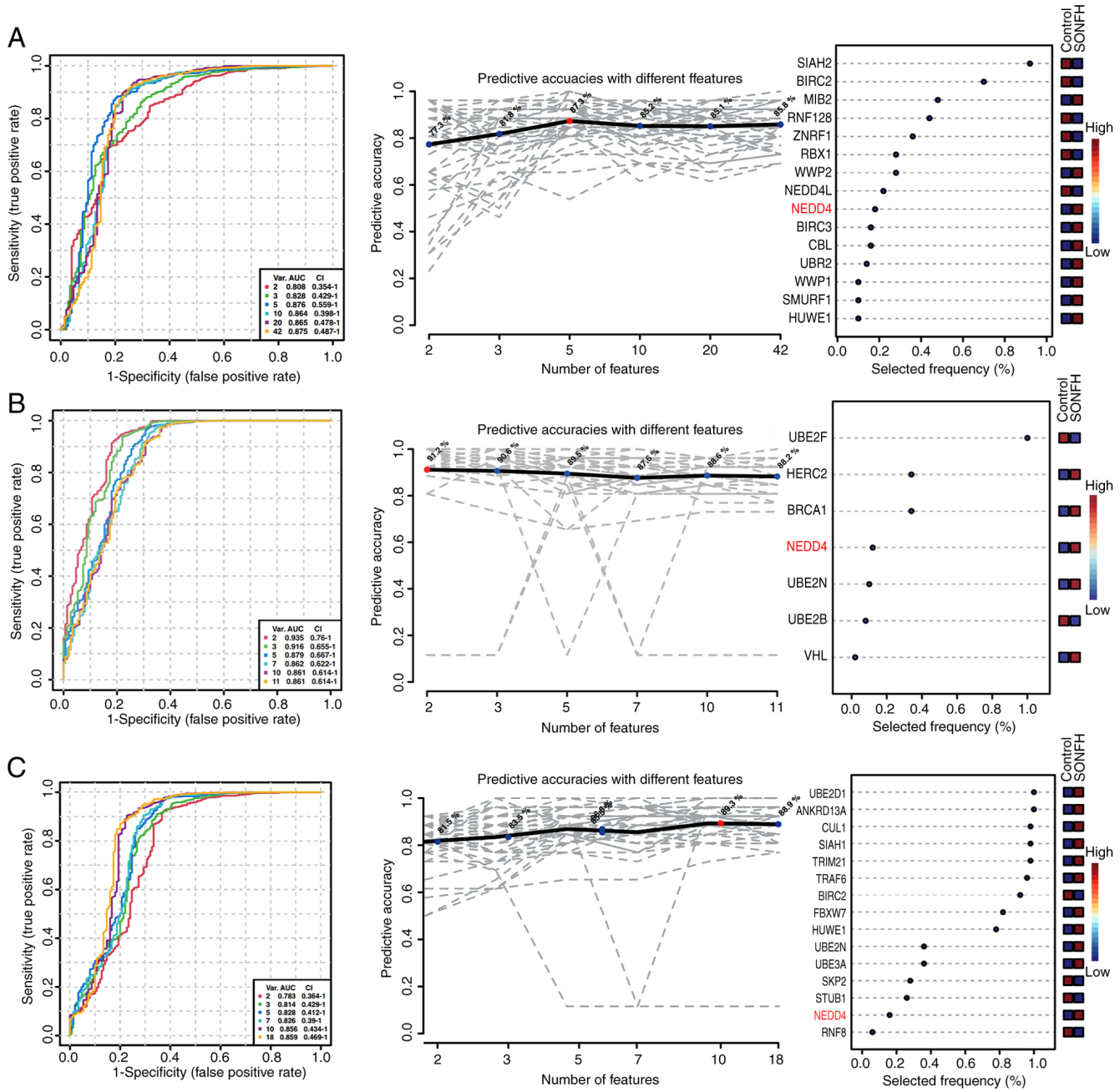

Figure 3. Multivariate exploratory ROC analysis of NEDD4 in SONFH. (A) ROC analysis, prediction accuracy and gene selection frequency for genes in the ubiquitin-ubiquitin ligase activity pathway. (B) ROC analysis, prediction accuracy and gene selection frequency for genes in the ubiquitin-mediated proteolysis pathway. (C) ROC analysis, prediction accuracy and gene selection frequency for genes in the positive regulation of protein ubiquitination pathway. ROC, receiver operating characteristic; AUC, area under the curve; Var., variables; SONFH, steroid-induced osteonecrosis of the femoral head; NEDD4, neural precursor cell expressed developmentally downregulated protein 4.

angiogenesis (Figs. 4C and S3). Within cell proliferation-related pathways, NEDD4 displayed significant positive correlations with multiple genes, including EIF4EBP1 (R=0.53), SAV1 (R=0.51), GDF11 (R=0.54) and MTOR (R=0.37), further highlighting the key role of NEDD4 in cell proliferation and metabolic regulation (Figs. 4D and S3). These findings indicated that NEDD4 serves an important role in regulating the cell cycle, angiogenesis and cell proliferation in SONFH.

OE of NEDD4 promotes proliferation, angiogenesis and wound healing in BMECs. To determine the role of NEDD4 in SONFH, a NEDD4 OE vector was created and tested in BMECs. BMECs displayed clear boundaries, no trailing and appeared healthy (Fig. 5A and B), following transfection with si-NEDD4 or si-NC. BMECs also remained in healthy condition, characterized by intact cell morphology, clear cell-cell boundaries and absence of cytoplasmic blebbing, following transient overexpression of NEDD4 (pcDNA3.1-NEDD4-3xHA) compared with the OE-NC group (Fig. 5C). RT-qPCR demonstrated significantly increased NEDD4 mRNA levels in the OE-NEDD4 group compared with the OE-NC group, indicating successful transfection (Fig. 5D). After 48 h, the optical

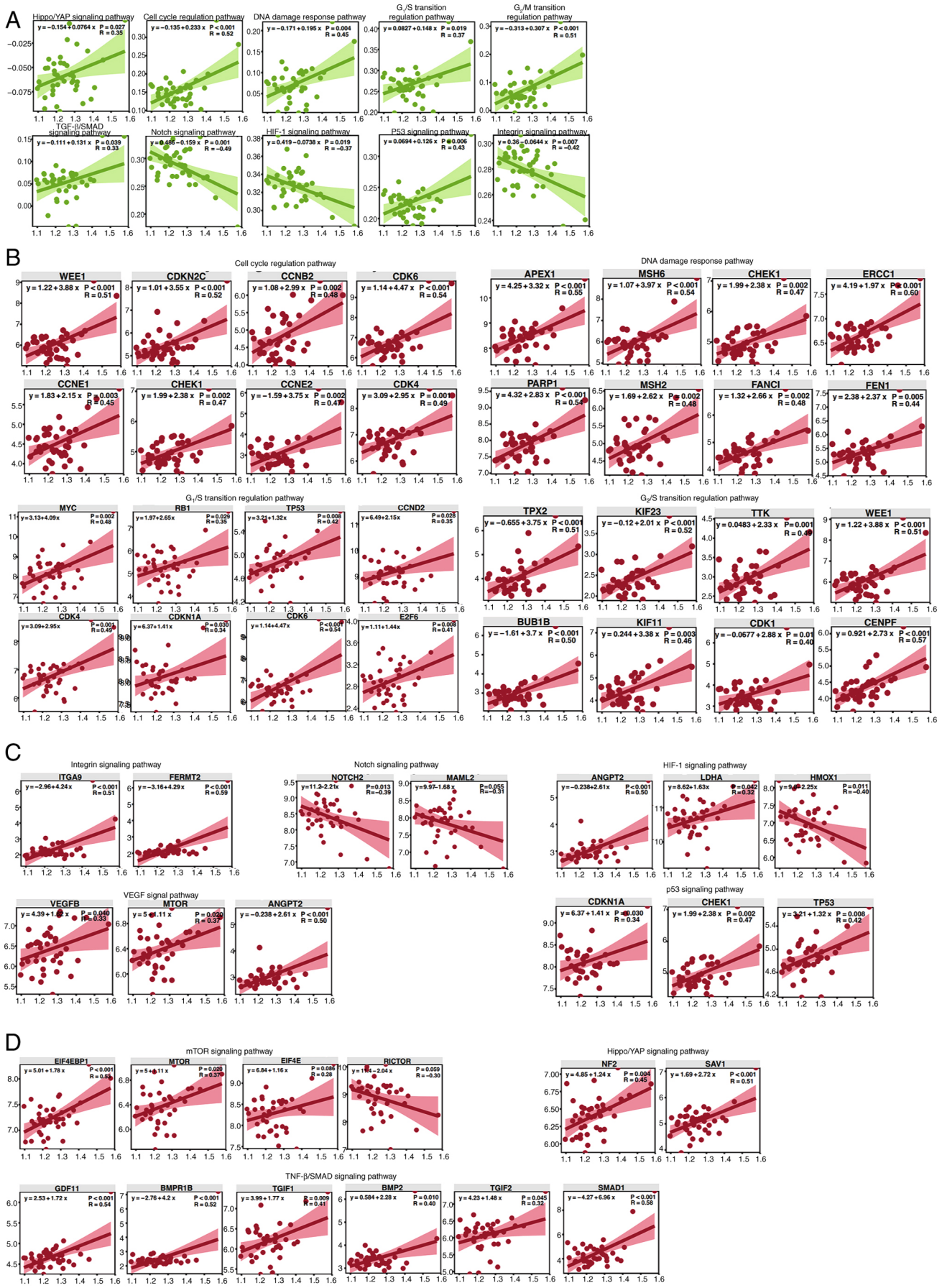

Figure 4. Key roles of NEDD4 in various biological pathways and its correlation with gene expression. (A) Correlation between NEDD4 and pathways related to cell proliferation, the cell cycle and angiogenesis. (B) Correlation between NEDD4 and cell cycle pathway genes. (C) Correlation between NEDD4 and angiogenesis pathway genes. (D) Correlation between NEDD4 and cell growth pathway genes. NEDD4, neural precursor cell expressed developmentally downregulated protein 4.

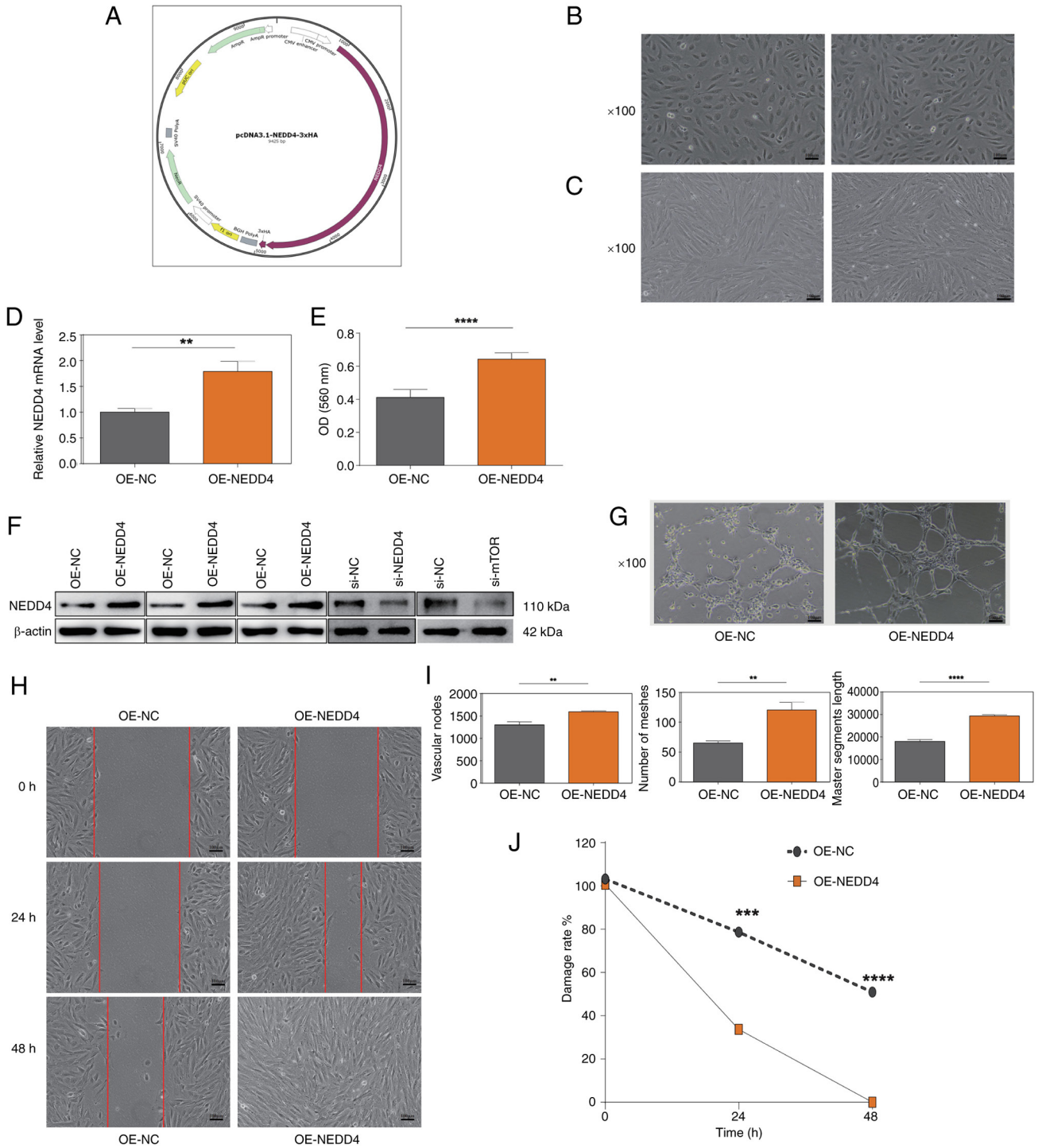

Figure 5. Effects of NEDD4 overexpression on BMECs. (A) Morphology of BMECs in the control group showing normal cell boundaries and morphology. (B) Morphology of BMECs in the OE-NEDD4 group showing no visible damage. (C) BMECs maintained good condition after transient NEDD4 transfection. Magnification, x100. (D) Reverse transcription-quantitative PCR confirmed significantly elevated NEDD4 mRNA expression in the OE-NEDD4 group. (E) An MTT assay showed increased viability of BMECs after NEDD4 overexpression. (F) Western blot analysis demonstrating efficient NEDD4 overexpression and knockdown in OE-NEDD4- and siRNA-2-transfected cells, respectively. (G) Quantitative analysis of tube formation indicating increased number of meshes, greater master segment length, and more vascular nodes in the OE-NEDD4 group. (H) Representative wound-healing assay showing smaller scratch areas in the OE-NEDD4 group. Magnification, x100; scale bar, 100 μm. (I) Quantitative analysis of wound-healing rates, indicating significantly improved migration capacity in the OE-NEDD4 group. (J) Decreased scratch area in the OE-NEDD4 group at 0, 24 and 48 h, consistent with enhanced migration ability. Magnification, x100. OE, overexpression; NC, negative control; si, small interfering RNA; NEDD4, neural precursor cell expressed developmentally downregulated protein 4; BMEC, bone microvascular endothelial cell; OD, optical density. *P<0.05; **P<0.01; ***P<0.001; ****P<0.0001 vs. OE-NC or 0 h.

density (OD)560 values of BMECs in the OE-NEDD4 group were significantly increased compared with those in the control group (Fig. 5E). Western blot analysis supported notable OE of NEDD4 in pcDNA3.1-NEDD4-3xHA-transfected BMECs compared with controls and effective knockdown of NEDD4 and mTOR in si-NEDD4- and si-mTOR-transfected cells, respectively. (Fig. 5F). The tube formation assay revealed a significant increase in the total tube length and number of

junctions and meshes in BMECs in the OE-NEDD4 group compared with the control group (Fig. 5G and I). The wound healing assay indicated a significant decrease in wound area in the OE-NEDD4 compared with the control group at 24 and 48 h (Fig. 5H). Subsequently, the present study evaluated how NEDD4 affected the viability of BMECs using an MTT assay; OE-NEDD4 group exhibited significantly higher OD (560 nm) values compared with the control group, indicating enhanced cell viability (Fig. 5J).

NEDD4 regulates vascular endothelial cell function by activating the VEGF signaling pathway while functionally interacting with mTOR signaling in BMECs. To verify the associations between NEDD4, mTOR and the VEGF signaling pathway, the present study used RT-qPCR to measure the mRNA levels of mTOR, VEGF and VEGFR2. NEDD4 OE significantly increased the mRNA levels of mTOR, VEGF and VEGFR2 (Fig. 6A). To explore the role of NEDD4 in BMEC function via mTOR regulation, siRNA transfection was performed to generate si-NEDD4- and si-mTOR-transfected BMECs. RT-qPCR identified si-NEDD4-1 and si-mTOR-3 as the most effective interference sequences (Fig. 6B). IP was performed to assess the ubiquitination level of mTOR, revealing a notable decrease in mTOR ubiquitination in NEDD4-overexpressing cells compared with the control group (Fig. 6C). .The morphology and fluorescence of BMECs following siRNA transfection confirmed successful transfection efficiency (Fig. 6D). Wound healing assay results showed a significant reduction in wound healing rates in the si-NEDD4 and si-mTOR groups compared with the control group, with a greater decrease observed in the si-NEDD4 + si-mTOR group at 48 h, aligning with the results from the MTT and EdU assays, where si-NEDD4 and si-NEDD4 + si-mTOR groups showed significantly reduced proliferation while the si-mTOR group exhibited a non-significant downward trend (Fig. 6E-G). In the tube formation assay, total tube length and number of junctions and meshes were significantly decreased in the si-NEDD4 and si-mTOR groups compared with the control group, with further significant reductions observed in the si-NEDD4 + si-mTOR group compared with the si-NEDD4 group, consistent with the findings from the MTT and scratch assays (Fig. 6H). In the MTT assay, OD560 values were significantly decreased in the si-NEDD4- and si-mTOR-transfected groups compared with the control group, and further decreased in the si-NEDD4 + si-mTOR compared with the si-NEDD4 group (Fig. 6I).

Glucocorticoids inhibit NEDD4 expression by upregulating methylation levels in its promoter region. Correlation analysis of NEDD4 and methylation-related genes showed significant positive and negative correlations with genes such as KDM6B, PCNA, DNMT3A, SUV39H2, UHRF1, EZH2, TET2, DMAP1 and PRMT1, further highlighting the complex role of NEDD4 in methylation regulation (Fig. 7A). BMECs exhibited healthy proliferation after treatment with PBS, MePr, 5-AZA, or MePr + 5-AZA (Fig. 7B). Methylation-specific PCR results revealed increased methylation levels following MePr addition and decreased levels following 5-AZA treatment. Compared with the 5-AZA group, combined treatment with MePr and 5-AZA increased methylation levels in the NEDD4 promoter region (Fig. 7C). RT-qPCR results indicated that combined treatment with MePr + 5-AZA significantly suppressed NEDD4 mRNA expression compared with 5-AZA treatment alone (Fig. 7D).

Discussion

Research highlights the important role of NEDD4 in ONFH. The p53 signaling pathway is important for regulating the cell cycle and apoptosis by slowing down cell proliferation and killing abnormal cells, while protecting healthy cells (34). P53 is controlled by post-translational modifications such as ubiquitination, phosphorylation, acetylation and methylation (34). The positive link between NEDD4 and the p53 signaling pathway, as well as tumor protein p53, suggests that NEDD4 may impact the cell cycle and apoptosis by affecting p53 activity (34). The DNA damage response (DDR) pathway is important for fixing DNA damage and preserving genome stability. When cellular DNA is harmed, the DDR pathway is activated, triggering cellular responses such as DNA repair (35,36). Important genes such as APEX1, MSH6, CHEK1, ERCC1, PARP1, MSH2, FANC and FEN1 are involved in DNA repair, influencing the cell cycle and apoptosis (37-42). The positive link between NEDD4 and key DDR genes suggests that NEDD4 may be involved in DNA repair and cell cycle control through its association with these genes. Additionally, CCNE1 and CCNE2 are regulatory subunits of CDK2 that control promote the re-entry of quiescent (G0-phase) cells into the cell cycle and regulate the G1/S phase transition (43). WEE1 encodes a kinase that negatively regulates the G_2/M transition of the cell cycle (44). Upregulation of this protein helps to strengthen the G_2/M DNA damage checkpoint (45). CHEK1 serves an important role in maintaining and restoring spermatogonial cells during mitosis (44). In meiosis, CHK1 selectively weakens the DNA damage signal on autosomes at specific stages, ensuring the normal progression of meiosis (46). The positive correlation between NEDD4 and cell cycle regulatory genes such as CCNE1, CCNE2, WEE1 and CHEK1 highlights its important role in the G_1/S and G_2/M transitions, as well as in mitosis and meiosis. In the present study, the significance of NEDD4 in cell cycle regulation and apoptosis was emphasized through its positive association with multiple key genes and signaling pathways. These results suggested that NEDD4 may serve an important role in the cell cycle and DNA damage repair in ONFH.

Integrins, as transmembrane receptors, can detect the physical properties of the extracellular matrix and organize the cytoskeleton while transmitting bidirectional cellular signals. They mediate signaling pathways such as the TGF-β, Hippo, Wnt and Notch pathways, thereby serving important roles in biological processes such as cell adhesion, spreading, migration and mechanotransduction (47,48). The Notch signaling pathway could have therapeutic benefits for bone regeneration and osteoporosis treatment (49). The analysis in the present study showed that NEDD4 expression was positively correlated with ssGSEA scores of the TGF-β/SMAD and Hippo/yes-associated protein (YAP) pathways but negatively correlated with the Notch signaling pathway. Although NEDD4 expression was positively correlated with ITGA9 and FERMT2 expression in the integrin pathway, the ssGSEA score for this pathway was negative, suggesting that the regulatory role of NEDD4

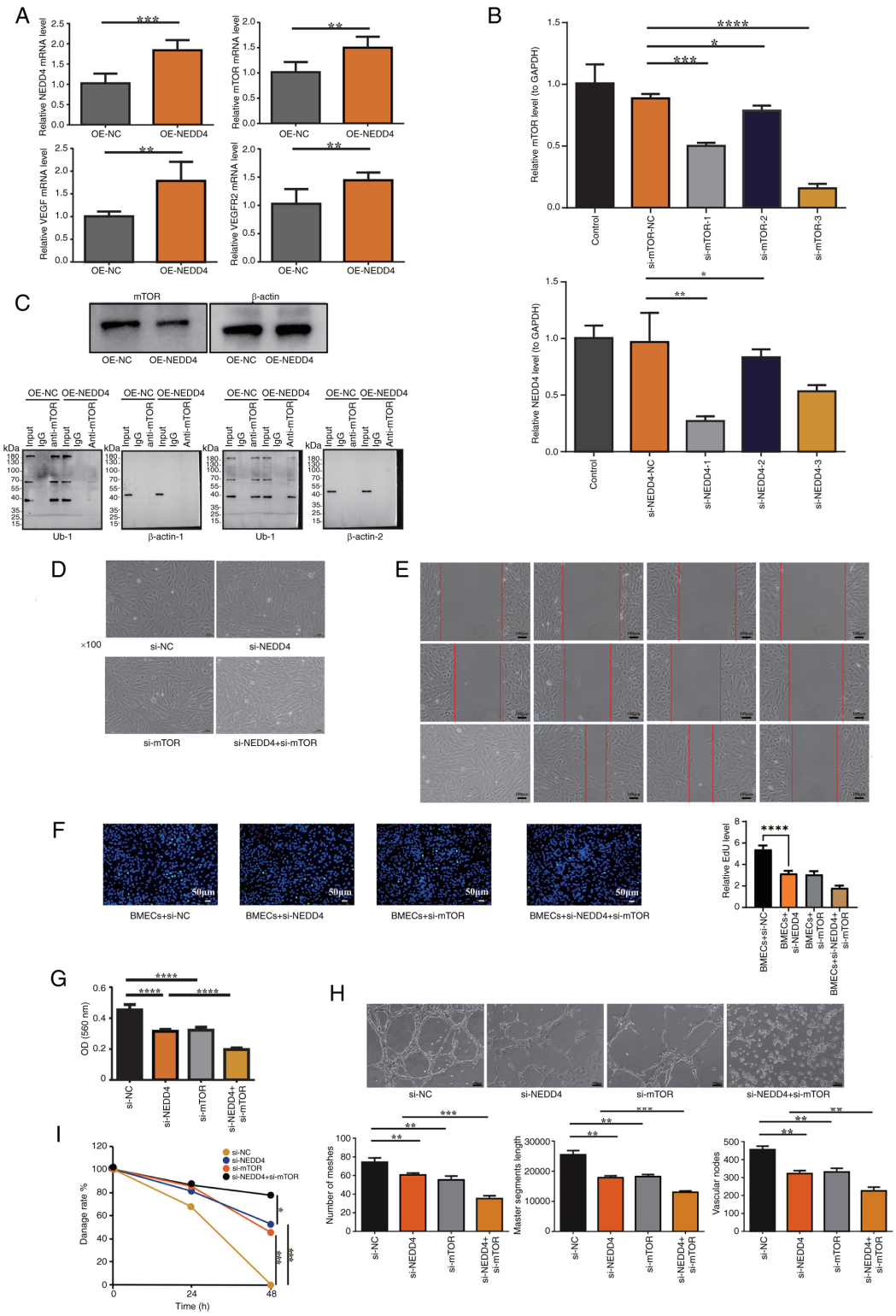

Figure 6. Functional validation of NEDD4 in the VEGF signaling pathway. (A) RT-qPCR showed increased mTOR, VEGF and VEGFR2 mRNA levels after NEDD4 overexpression. (B) RT-qPCR identified si-NEDD4-1 and si-mTOR-3 as the most effective interference sequences. (C) Immunoprecipitation analysis showing that NEDD4 overexpression decreased the ubiquitination level of mTOR. (D) Validation of transfection efficiency in BMECs. Representative microscopic images show cells transfected with si-NEDD4, si-mTOR and their respective controls (si-NC). BMECs maintained a normal morphology and healthy growth state after transfection, without observable cytotoxicity or detachment, confirming that the transfection was effective and did not adversely affect cell viability. Magnification, x100. (E) Scratch assay showing decreased wound closure rates in the si-NEDD4 and si-mTOR groups compared with the control group, with the lowest migration observed in the si-NEDD4 + si-mTOR group. Scale bar, 100 μm. (F) Representative images from the EdU proliferation assay demonstrating reduced EdU-positive nuclei in the si-NEDD4 and si-mTOR groups, with further reductions in the si-NEDD4 + si-mTOR group. Scale bar, 50 μm. (G) MTT assay showed reduced viability in si-NEDD4 and si-mTOR groups, with the greatest reduction in the si-NEDD4 + si-mTOR group. (H) Tube formation assay demonstrating reduced angiogenesis parameters in the si-NEDD4 and si-mTOR groups, with further reductions in the si-NEDD4 + si-mTOR group. Magnification, x100. (I) Quantitative analysis of wound-healing rates, indicating significantly reduced migration ability in the si-NEDD4 and si-mTOR groups, with further reduction in the si-NEDD4 + si-mTOR group. NC, negative control; si, small interfering RNA; NEDD4, neural precursor cell expressed developmentally downregulated protein 4; OE, overexpression; RT-qPCR, reverse transcription-quantitative PCR; BMEC, bone microvascular endothelial cell; OD, optical density; Ub-1, first ubiquitination site assay. *P<0.05, **P<0.01, ***P<0.001 and ****P<0.0001.

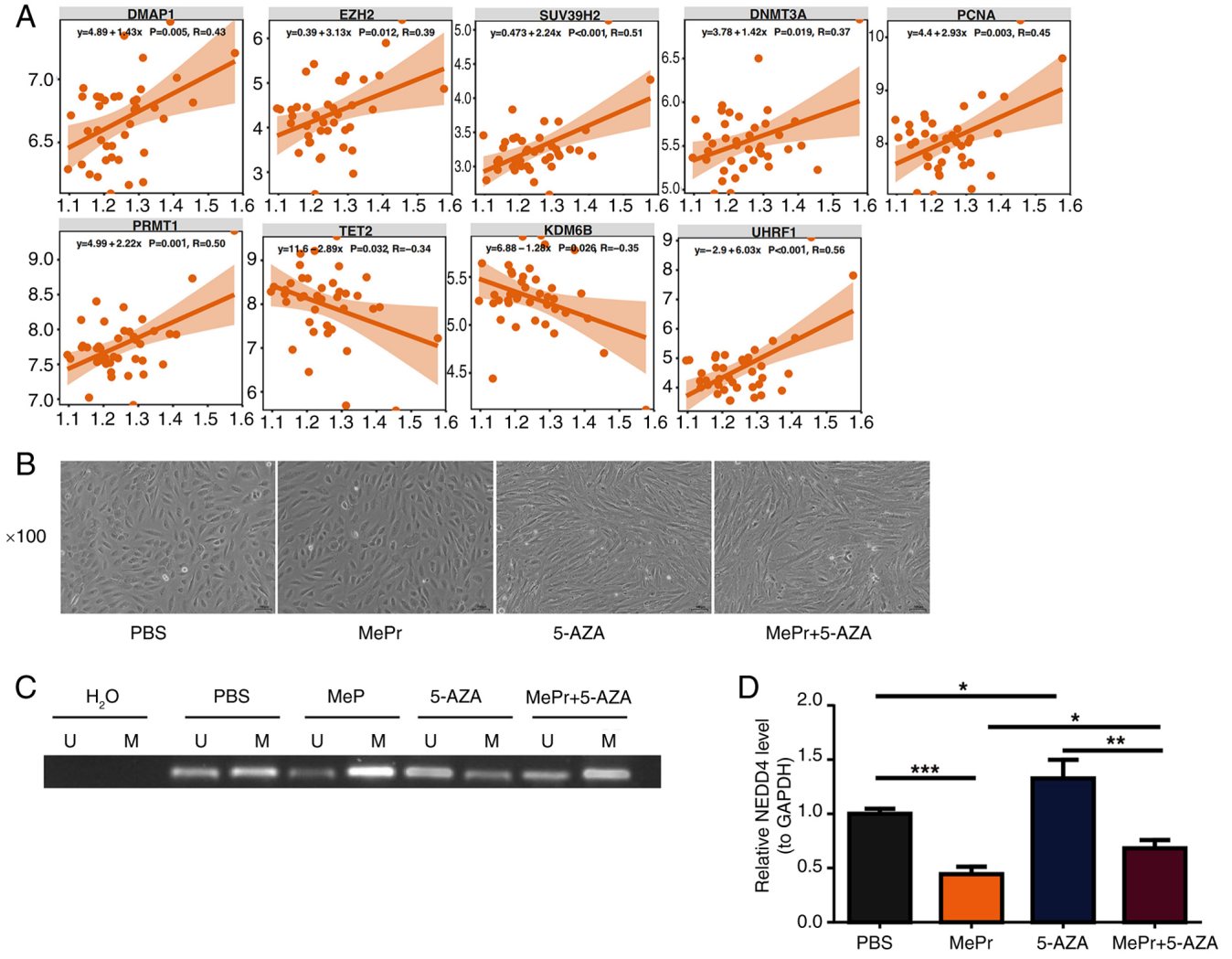

Figure 7. Glucocorticoids inhibit NEDD4 expression by increasing promoter methylation levels in BMECs. (A) Correlation between NEDD4 and methylation-related genes, with significance and correlation marked. (B) BMEC culture, including PBS, MePr, 5-AZA and MePr + 5-AZA groups. Magnification, x100. (C) Methylation PCR, with H_2O as the system negative control to exclude contamination. (D) NEDD4 mRNA expression level, with significant differences marked. U, unmethylated control; M, methylated sample; NEDD4, neural precursor cell expressed developmentally downregulated protein 4; BMEC, bone microvascular endothelial cell; MePr, methylprednisolone; 5-AZA, 5-azacytidine. *P<0.05, **P<0.01 and ***P<0.001.

is complex and this may influence pathways through different mechanisms. As an E3 ubiquitin ligase, NEDD4 may serve a key role in the progression and repair of ONFH. NEDD4 may contribute to bone tissue repair and remodeling by boosting the activity of the TGF-β/SMAD and Hippo/YAP signaling pathways (25,31). For example, NEDD4 may promote the growth and differentiation of bone cells by stabilizing TGF-β receptors or SMAL proteins (31). At the same time, by enhancing the Hippo/YAP pathway, it may help regulate the mechanical adaptability and repair of bone tissue (25). Conversely, the negative correlation between NEDD4 and the Notch signaling pathway genes such as NOTCH2 and MAML2 indicated that NEDD4 may affect the pathological process of SONFH by inhibiting the Notch pathway and influencing osteoblast differentiation (49). The interaction of the integrin signaling pathway with NEDD4 could impact the regulation of these pathways, further affecting the progression and repair of SONFH (47). In summary, the regulatory roles of NEDD4 in the integrin, TGF-β/SMAD, Hippo/YAP and Notch signaling pathways highlighted its complex function in cell signal transduction. This diverse regulatory mechanism offers important insights for further exploring the functions and mechanisms of NEDD4 in SONFH.

Research has shown that ANGPT2 serves an important role in the vascular niche within the bone marrow, helping to maintain the balance and regeneration of hematopoietic stem cells (50). Although VEGFB does not directly contribute to angiogenesis, it indirectly supports vascular growth and cell survival by affecting the actions of VEGFA (51). Bone morphogenetic protein receptor type-1B (BMPR1B) also serves a role, as it can prevent chondrocyte hypertrophy and act as a stabilizer for cartilage during joint development (52). mTOR is involved in tissue regeneration across neurons, muscles, liver and intestines, helping restore tissue homeostasis (53). In the present study, NEDD4 expression was positively associated with the expression of genes involved in angiogenesis, such as ANGPT2, VEGFB, MTOR and BMPR1B. This finding further emphasizes the notable role of NEDD4 in regulating both angiogenesis and bone tissue homeostasis. Notably, the positive correlation between NEDD4 and ANGPT2 supported

the role of ANGPT2 in coordinating hematopoietic stem cell homeostasis within the vascular niche (50). Additionally, this correlation suggested that NEDD4 may indirectly affect the function of VEGFA through interactions with VEGFB and mTOR, thereby encouraging vascular growth, and cell proliferation and survival (51,53). The positive correlation between NEDD4 and BMPR1B suggested that NEDD4 may prevent chondrocyte hypertrophy and support cartilage health and stability (52).

The present study demonstrated that NEDD4 OE promoted the viability, migration and angiogenesis of BMECs, indicating its key role in endothelial cell function, and maintaining angiogenesis and homeostasis. NEDD4 regulates processes such as proliferation and angiogenesis via ubiquitination (23). Glucocorticoid-induced apoptosis of BMECs promotes the onset and progression of ONFH (54). The present research sheds light on the role and mechanism of NEDD4 in ONFH. The present study found that NEDD4 enhanced the cell function of BMECs by activating the VEGF signaling pathway and working with mTOR. When NEDD4 was overexpressed, the mRNA levels of mTOR, VEGF and VEGFR2 were significantly increased, demonstrating that NEDD4 promoted angiogenesis by triggering the VEGF signaling pathway. Notably, overexpression of NEDD4 did not markedly affect the ubiquitination level of mTOR, suggesting that NEDD4 did not directly mediate the ubiquitination of mTOR but instead affected it by activating the mTOR signaling pathway. In the siRNA transfection experiments, a synergistic effect of NEDD4 and mTOR on BMEC proliferation and migration was observed. Additionally, glucocorticoids inhibited the expression of NEDD4 by increasing the methylation level of the NEDD4 promoter region. After adding the methylation inhibitor 5-AZA, the methylation levels of the NEDD4 promoter notably decreased, while glucocorticoid MePr treatment markedly increased the methylation level of the NEDD4 promoter and significantly suppressed NEDD4 mRNA expression. This further supported the important role of NEDD4 in methylation regulation and showed the substantial influence of glucocorticoids on NEDD4 expression.

In conclusion, the present study revealed the diverse roles of NEDD4 in SONFH, particularly in angiogenesis, cellular homeostasis, cell cycle regulation and DNA damage repair. NEDD4 enhanced BMEC function by activating the VEGF signaling pathway and working with mTOR, with its expression regulated by methylation. This offers novel insights into NEDD4 as a potential therapeutic target for SONFH. Further research into the functions of NEDD4 in bone pathology and angiogenesis will provide valuable insights for developing novel treatment strategies. These findings not only add to the existing literature but also provide novel perspectives on the multiple roles of NEDD4 in SONFH and angiogenesis, indicating that NEDD4 may affect angiogenesis, bone tissue repair and bone regeneration through various mechanisms.

NEDD4 may represent a promising therapeutic target for SONFH. By mediating PTEN degradation and activating the PI3K/AKT/mTOR pathway, NEDD4 promoted cell proliferation and survival, while also enhancing VEGF signaling to support angiogenesis and bone repair (26,31). These dual effects on osteogenesis and angiogenesis highlight its translational potential, and future studies on pharmacological or genetic modulation of NEDD4 could lead to novel treatment strategies.

The present study had several limitations. Primarily, the bioinformatics analysis was based on a single publicly available dataset without external validation, which may limit the generalizability of the present findings. Secondly, although the present study validated key molecular alterations *in vitro*, *in vivo* animal experiments were not performed, which reduced the translational value of the results. Furthermore, the relatively small sample size and limited types of control may weaken the conclusions of the present study. Additionally, the present study did not explore how NEDD4 regulates the mTOR and VEGF pathways at a mechanistic level. Finally, the present study did not include clinical relevance data, and thus, future studies should incorporate patient samples and correlation analyses to increase the translational significance of the present work. Overall, future research with larger cohorts, more comprehensive controls, *in vivo* validation, more in-depth mechanistic studies and clinical correlation analyses is needed to confirm and extend the findings of the present study.

Acknowledgements

Not applicable.

Funding

The present study was funded by The Guizhou Provincial Natural Science Foundation [grant no. Qiankehebasis-ZK (2024) general 241], the Start-up Fund for Doctoral Research at the Affiliated Hospital of Guizhou Medical University (grant no. gyfybsky-2022-38), the National Natural Science Foundation of China Cultivation Program of Affiliated Hospital of Guizhou Medical University [grant no. gyfynsfc(2023)-62], the Key Medical Discipline Construction Project of Guizhou Provincial Health Commission during 2025-2026, and the 2025 Annual Hospital-Level Scientific Research Fund of Guizhou Hospital of Beijing Jishuitan Hospital [grant no. JGYYK(2025)-24].

Availability of data and materials

The data generated in the present study may be requested from the corresponding author.

Authors' contributions

JL conceived and designed the experiments, performed the experiments, analyzed the data, authored and reviewed drafts of the article, and approved the final draft. DZ performed the experiments. YQ analyzed and interpreted data CG supervised the study and interpreted data. All authors read and approved the final version of the manuscript, JL and CG confirm the authenticity of all the raw data.

Ethics approval and consent to participate

The use of primary human cells in the present study was conducted in accordance with The Declaration of Helsinki. The protocol was approved by the Ethics Committee of

Beijing Jishuitan Hospital Guizhou Hospital (approval no. KT2025022804; Guiyang, China).

Patient consent for publication

Not applicable.

Competing interests

The authors declare that they have no competing interests.

References

1. Zhang W, Du H, Liu Z, Zhou D, Li Q and Liu W: Worldwide research trends on femur head necrosis (2000-2021): A bibliometrics analysis and suggestions for researchers. Ann Transl Med 11: 155, 2023.
2. Wang T, Azeddine B, Mah W, Harvey EJ, Rosenblatt D and Séguin C: Osteonecrosis of the femoral head: Genetic basis. Int Orthop 43: 519-530, 2019.
3. Shao W, Wang P, Lv X, Wang B, Gong S and Feng Y: Unraveling the role of endothelial dysfunction in osteonecrosis of the femoral head: A pathway to new therapies. Biomedicines 12: 664, 2024.
4. Fukushima W, Fujioka M, Kubo T, Tamakoshi A, Nagai M and Hirota Y: Nationwide epidemiologic survey of idiopathic osteonecrosis of the femoral head. Clin Orthop Relat Res 468: 2715-2724, 2010.
5. Mont MA, Pivec R, Banerjee S, Issa K, Elmallah RK and Jones LC: High-dose corticosteroid use and risk of hip osteonecrosis: Meta-analysis and systematic literature review. J Arthroplasty 30: 1506-1512.e5, 2015.
6. Radke S, Battmann A, Jatzke S, Eulert J, Jakob F and Schütze N: Expression of the angiomatrix and angiogenic proteins CYR61, CTGF, and VEGF in osteonecrosis of the femoral head. J Orthop Res 24: 945-952, 2006.
7. Shao W, Li Z, Wang B, Gong S, Wang P, Song B, Chen Z and Feng Y: Dimethyloxalylglycine attenuates steroid-associated endothelial progenitor cell impairment and osteonecrosis of the femoral head by regulating the HIF-1α signaling pathway. Biomedicines 11: 992, 2023.
8. Huard J: Stem cells, blood vessels, and angiogenesis as major determinants for musculoskeletal tissue repair. J Orthop Res 37: 1212-1220, 2019.
9. Wang Y, Xia CJ, Wang BJ, Ma XW and Zhao DW: The association between VEGF-634C/G polymorphisms and osteonecrosis of femoral head: A meta-analysis. Int J Clin Exp Med 8: 9313-9319, 2015.
10. Hang D, Wang Q, Guo C, Chen Z and Yan Z: Treatment of osteonecrosis of the femoral head with VEGF165 transgenic bone marrow mesenchymal stem cells in mongrel dogs. Cells Tissues Organs 195: 495-506, 2012.
11. Grosso A, Burger MG, Lunger A, Schaefer DJ, Banfi A and Di Maggio N: It takes two to tango: Coupling of angiogenesis and osteogenesis for bone regeneration. Front Bioeng Biotechnol 5: 68, 2017.
12. Portal-Núñez S, Lozano D and Esbrit P: Role of angiogenesis on bone formation. Histol Histopathol 27: 559-566, 2012.
13. Deng S, Xiang JJ, Shen YY, Lin SY, Zeng YQ and Shen JP: Effects of VEGF-notch signaling pathway on proliferation and apoptosis of bone marrow MSC in patients with aplastic anemia. Zhongguo Shi Yan Xue Ye Xue Za Zhi 27: 1925-1932, 2019 (In Chinese).
14. Wang S, Lu J, You Q, Huang H, Chen Y and Liu K: The mTOR/AP-1/VEGF signaling pathway regulates vascular endothelial cell growth. Oncotarget 7: 53269-53276, 2016.
15. Liu Z and Li Y: Expression of the HIF-1α/VEGF pathway is upregulated to protect alveolar bone density reduction in nasal-obstructed rats. Histol Histopathol 39: 1053-1063, 2024.
16. Gao L, Zhang W, Shi XH, Chang X, Han Y, Liu C, Jiang Z and Yang X: The mechanism of linear ubiquitination in regulating cell death and correlative diseases. Cell Death Dis 14: 659, 2023.
17. Popovic D, Vucic D and Dikic I: Ubiquitination in disease pathogenesis and treatment. Nat Med 20: 1242-1253, 2014.
18. Wang Y, Huang S, Xu P and Li Y: Progress in atypical ubiquitination via K6-linkages. Sheng Wu Gong Cheng Xue Bao 38: 3215-3227, 2022 (In Chinese).
19. Yan J, Qiao G, Yin Y, Wang E, Xiao J, Peng Y, Yu J, Du Y, Li Z, Wu H, *et al*: Black carp RNF5 inhibits STING/IFN signaling through promoting K48-linked ubiquitination and degradation of STING. Dev Comp Immunol 145: 104712, 2023.
20. Xu J, Sheng Z, Li F, Wang S, Yuan Y, Wang M and Yu Z: NEDD4 protects vascular endothelial cells against Angiotensin II-induced cell death via enhancement of XPO1-mediated nuclear export. Exp Cell Res 383: 111505, 2019.
21. Eide PW, Cekaite L, Danielsen SA, Eilertsen IA, Kjenseth A, Fykerud TA, Ågesen TH, Bruun J, Rivedal E, Lothe RA and Leithe E: NEDD4 is overexpressed in colorectal cancer and promotes colonic cell growth independently of the PI3K/PTEN/AKT pathway. Cell Signal 25: 12-18, 2013.
22. Huang ZJ, Zhu JJ, Yang XY and Biskup E: NEDD4 promotes cell growth and migration via PTEN/PI3K/AKT signaling in hepatocellular carcinoma. Oncol Lett 14: 2649-2656, 2017
23. Guo Y, Wang Y, Liu H, Jiang X and Lei S: High glucose environment induces NEDD4 deficiency that impairs angiogenesis and diabetic wound healing. J Dermatol Sci 112, 148-157, 2023.
24. Sun W, Lu H, Cui S, Zhao S, Yu H, Song H, Ruan Q, Zhang Y, Chu Y and Dong S: NEDD4 ameliorates myocardial reperfusion injury by preventing macrophages pyroptosis. Cell Commun Signal 21: 29, 2023.
25. Xu K, Chu Y, Liu Q, Fan W, He H and Huang F: NEDD4 E3 Ligases: Functions and mechanisms in bone and tooth. Int J Mol Sci 23: 9937, 2022.
26. Drinjakovic J, Jung H, Campbell DS, Strochlic L, Dwivedy A and Holt CE: E3 ligase Nedd4 promotes axon branching by downregulating PTEN. Neuron 65: 341-357, 2010.
27. Han X, Zhang G, Chen G, Wu Y, Xu T, Xu H, Liu B and Zhou Y: Buyang huanwu decoction promotes angiogenesis in myocardial infarction through suppression of PTEN and activation of the PI3K/Akt signalling pathway. J Ethnopharmacol 287: 114929, 2022.
28. Zhou YJ, Xiong YX, Wu XT, Shi D, Fan W, Zhou T, Li YC and Huang X: Inactivation of PTEN is associated with increased angiogenesis and VEGF overexpression in gastric cancer. World J Gastroenterol 10: 3225-3229, 2004.
29. Lindberg ME, Stodden GR, King ML, MacLean JA II, Mann JL, DeMayo FJ, Lydon JP and Hayashi K: Loss of CDH1 and Pten accelerates cellular invasiveness and angiogenesis in the mouse uterus. Biol Reprod 89: 8, 2013.
30. Jeon SA, Lee JH, Kim DW and Cho JY: E3-ubiquitin ligase NEDD4 enhances bone formation by removing TGFβ1-induced pSMAD1 in immature osteoblast. Bone 116: 248-258, 2018.
31. Zheng HL, Xu WN, Zhou WS, Yang RZ, Chen PB, Liu T, Jiang LS and Jiang SD: Beraprost ameliorates postmenopausal osteoporosis by regulating Nedd4-induced Runx2 ubiquitination. Cell Death Dis 12: 497, 2021.
32. Livak KJ and Schmittgen TD: Analysis of relative gene expression data using real-time quantitative PCR and the 2(-Delta Delta C(T)) method. Methods 25: 402-408, 2001.
33. Liang XZ, Luo D, Chen YR, Li JC, Yan BZ, Guo YB, Wen MT, Xu B and Li G: Identification of potential autophagy-related genes in steroid-induced osteonecrosis of the femoral head via bioinformatics analysis and experimental verification. J Orthop Surg Res. 17: 86, 2022.
34. Liu Y, Su Z, Tavana O and Gu W: Understanding the complexity of p53 in a new era of tumor suppression. Cancer Cell 42: 946-967, 2024.
35. Chatterjee N and Walker GC: Mechanisms of DNA damage, repair, and mutagenesis. Environ Mol Mutagen 58: 235-263, 2017.
36. Ciccia A and Elledge SJ: The DNA damage response: Making it safe to play with knives. Mol Cell 40: 179-204, 2010.
37. Li J, Zhao H, McMahon A and Yan S: APE1 assembles biomolecular condensates to promote the ATR-Chk1 DNA damage response in nucleolus. Nucleic Acids Res 50: 10503-10525, 2022.
38. Provasek V, Kodavati M, Kim B, Mitra J and Hegde ML: TDP43 Interacts with MLH1 and MSH6 Proteins in A DNA Damage-Inducible Manner. Mol Brain 17: 32, 2024.
39. Pfeiffer C, Grandits AM, Asnagli H, Schneller A, Huber J, Zojer N, Schreder M, Parker AE, Bolomsky A, Beer PA and Ludwig H: CTPS1 is a novel therapeutic target in multiple myeloma which synergizes with inhibition of CHEK1, ATR or WEE1. Leukemia 38: 181-192, 2024.
40. Li WH, Wang F, Song GY, Yu QH, Du RP and Xu P: PARP-1: A critical regulator in radioprotection and radiotherapy-mechanisms, challenges, and therapeutic opportunities. Front Pharmacol 14: 1198948, 2023.

41. Olazabal-Herrero A, He B, Kwon Y, Gupta AK, Dutta A, Huang Y, Boddu P, Liang Z, Liang F, Teng Y, *et al*: The FANCI/FANCD2 complex links DNA damage response to R-loop regulation through SRSF1-mediated mRNA export. Cell Rep 43: 113610, 2024.
42. Zheng L, Jia J, Finger LD, Guo Z, Zer C and Shen B: Functional regulation of FEN1 nuclease and its link to cancer. Nucleic Acids Res 39: 781-794, 2011.
43. Sonntag R, Giebeler N, Nevzorova YA, Bangen JM, Fahrenkamp D, Lambertz D, Haas U, Hu W, Gassler N, Cubero FJ, *et al*: Cyclin E1 and cyclin-dependent kinase 2 are critical for initiation, but not for progression of hepatocellular carcinoma. Proc Natl Acad Sci USA 115: 9282-9287, 2018.
44. Ghelli Luserna di Rorà A, Cerchione C, Martinelli G and Simonetti G: A WEE1 family business: Regulation of mitosis, cancer progression, and therapeutic target. J Hematol Oncol 13: 126, 2020.
45. Sokhi S, Lewis CW, Bukhari AB, Hadfield J, Xiao EJ, Fung J, Yoon YJ, Hsu WH, Gamper AM and Chan GK: Myt1 overexpression mediates resistance to cell cycle and DNA damage checkpoint kinase inhibitors. Front Cell Dev Biol 11: 1270542, 2023.
46. Abe H, Alavattam KG, Kato Y, Castrillon DH, Pang Q, Andreassen PR and Namekawa SH: CHEK1 coordinates DNA damage signaling and meiotic progression in the male germline of mice. Hum Mol Genet 27: 1136-1149, 2018.
47. Li S, Sampson C, Liu C, Piao HL and Liu HX: Integrin signaling in cancer: Bidirectional mechanisms and therapeutic opportunities. Cell Commun Signal 21: 266, 2023.
48. Huveneers S and Danen EH: Adhesion signaling-crosstalk between integrins, Src and Rho. J Cell Sci 122: 1059-1069, 2009.
49. Nobta M, Tsukazaki T, Shibata Y, Xin C, Moriishi T, Sakano S, Shindo H and Yamaguchi A: Critical regulation of bone morphogenetic protein-induced osteoblastic differentiation by Delta1/Jagged1-activated Notch1 signaling. J Biol Chem 280: 15842-15848, 2005.
50. Rafii S and Lis R: Angiocrine ANGPTL2 executes HSC functions in endothelial niche. Blood 139: 1433-1434, 2022.
51. Lal N, Puri K and Rodrigues B: Vascular endothelial growth factor B and its signaling. Front Cardiovasc Med 5: 39, 2018.
52. Mang T, Kleinschmidt-Doerr K, Ploeger F, Schoenemann A, Lindemann S and Gigout A: BMPR1A is necessary for chondrogenesis and osteogenesis, whereas BMPR1B prevents hypertrophic differentiation. J Cell Sci 133: jcs246934, 2020.
53. Wei X, Luo L and Chen J: Roles of mTOR signaling in tissue regeneration. Cells 8: 1075, 2019.
54. Zhang F, Wei L, Wang L, Wang T, Xie Z, Luo H, Li F, Zhang J, Dong W, Liu G, *et al*: FAR591 promotes the pathogenesis and progression of SONFH by regulating Fos expression to mediate the apoptosis of bone microvascular endothelial cells. Bone Res 11: 27, 2023.